Reprinted from JOURNAL OF CATALYSIS, Volume 18, Number 2, August 1970

JOURNAL OF CATALYSIS 18, 164–183 (1970)

Disproportionation of CO

I. Over Iron and Silicon-Iron Single Crystals

G. D. RENSHAW, C. ROSCOE, AND P. L. WALKER, JR.

Department of Materials Science, Pennsylvania State University, University Park, Pennsylvania 16802

Received September 11, 1969

A detailed study of the catalytic disproportionation of CO over Fe and 3.5% Si–Fe single crystals in the range 550-800°C has been made. For both Fe and Si–Fe it has been demonstrated that γ-Fe_2O_3 is the active catalytic species. It is considered that the defect type structure associated with this oxide aids the diffusion of Fe^{3+} ions to the surface where they may facilitate the breakdown of CO molecules. The notable reduction in rate of reaction at temperatures above 550°C was shown to be a direct result of the formation of α-Fe_2O_3 in which the diffusion of Fe^{3+} ions is considerably less than in γ-Fe_2O_3.

Electron microscopy and selected area diffraction studies of the highly fibrous carbonaceous products formed at various stages in the reaction revealed that at 550°C the reaction proceeds via the breakdown of Fe_3C whiskers (predominately) and platelets. The overall reaction is discussed in terms of the conditions necessary for the formation of the particular Fe oxides and the growth and reactions of Fe carbides.

INTRODUCTION

The catalytic disproportionation of carbon monoxide to carbon and carbon dioxide has received wide spread attention (*1–5*) because of its importance in many industrial processes. A bibliography, up to 1956, of the literature and patents related to the production of carbon by this reaction is available (*6*). In the gas cooled high temperature reactor, small amounts of CO formed in the high temperature region disproportionate catalytically in the cooler (ca. 550°C) heat exchanger region with the ultimate corrosion of the heat exchanger walls. This type of corrosion is generally termed "metal dusting" (*7*). Undesirable carbon deposition also occurs as a side reaction in the low temperature reduction of ores and in the synthesis of hydrocarbons by the Fischer-Tropsch process where the reaction may lead to the deactivation of the catalyst. Disintegration of furnace linings also has been attributed to carbon deposition at iron oxide impurities in the fireclay brick.

The most active catalysts for the reaction are the ferromagnetic metals Fe, Co, and Ni. For Fe catalysis in particular, the precise catalytic mechanism is not known, although many suggestions have been proffered. A representative cross section of the principal conclusions reached by some of the previous investigators are listed chronologically in Table 1. The confusion regarding the nature of the catalytic species is understandable when one considers the complexity of the system and also that most of the studies have been carried out with finely divided powdered catalysts.

It appears likely that the stoichiometric equation,

$$2CO \rightleftharpoons C + CO_2, \qquad (1)$$

merely approximates to the overall reaction, whereas the final products actually result from a sequence of intermediate reactions. Depending on the experimental conditions, the latter could involve any one of a series of oxides or carbides, or even a combination of both. In this respect, it is perhaps significant that readily detectable rates of

TABLE 1
SUMMARY OF SOME PREVIOUS INVESTIGATIONS

Investigators	Year	Proposed Catalyst or Mechanism
Boudouard (*8*)	1901	Iron oxides
Hilpert and Dieckmann (*9*)	1915	Cementite (Fe_3C)
Hofmann and Groll (*10*)	1928	Fe
Tutiya (*11*)	1929	Fe_3C
Olmer (*12*)	1941	Fe
Baukloh and Edwin (*13*)	1942	Fe
Fleureau (*14*)	1953	Formation of Fe carbonyls as the first step in reaction. Decomposition of these gave free carbon and Fe which could then repeat the cycle.
Chatterjee and Das (*15*)	1954	Fe
Taylor (*2*)	1956	Formation of an iron–iron oxide interface at which point carbon could enter the Fe lattice because of the larger lattice spacings in the vicinity of the interface.
Berry *et al.* (*1*)	1956	Hagg carbide (Fe_2C) from 400 to 565°C and a form of Fe_3C, having an abnormally low Curie temperature, from 565 to 700°C.
Walker *et al.* (*3*, *4*)	1959	Suggested Fe as the catalyst since CO can chemisorb on Fe but not on Fe_3C. Thus reaction stops when all the Fe has been converted to the latter.
MacRae (*16*)	1966	Iron–iron oxide interface
Haas *et al.* (*5*)	1968	Fe
Ruston *et al.* (*17*)	1969	Fe_7C_3 and Fe

disproportionation are found only when H_2 (*3*, *4*) or, alternatively, water vapor (*5*) are introduced in to the gas stream. It would appear that H_2 could modify the catalytic mode both directly, by promoting the rupture of the C–O bond and indirectly, by regenerating for instance a completely carbided catalyst which in this situation is regarded as being inactive (*4*). When present in a sufficient quantity, water vapor would lead to the oxidation of the Fe surfaces.

Special mention is now made of a few studies selected because of their particular relevance to the following discussion. Taylor (*2*) noted that when powdered Fe was employed as the catalyst, magnetite (Fe_3O_4) was always present in the reaction products. Further, he found that the catalytic activity of a series of iron oxides was very dependent upon the following factors:

(i) the method of preparation of the iron oxide,

(ii) its purity,

(iii) the aging time and heat treatment the oxide was subjected to.

Taylor suggested that the mechanism for disproportionation involved an Fe–Fe_3O_4 interface. It was supposed that the mismatch in lattice spacings at this interface favored the migration of carbon atoms into the ferrite lattice. Then at high levels of carbon supersaturation, obtained with an active catalyst, a metastable carbide was assumed to form, so deactivating the catalyst. For the lower supersaturation levels associated with a less active catalyst, graphite was said to constitute the primary solid product.

Earlier Trillat and Oketani (*18–19*) had observed the formation of Fe_3O_4 during a transmission electron diffraction study of the cementation of polycrystalline Fe films at 550°C in a CO atmosphere. However, in a subsequent study employing Fe single crystals, Kehrer and Leidheiser (*20*) determined the presence of Fe_3O_4, by a glancing angle X-ray diffraction technique, only on

the surface of specimens treated with CO below 350°C. The other primary product at this temperature was Hägg carbide (Fe_2C). On a crystal surface exposed to CO at 550°C, prior to carbon formation, the latter authors noted the formation of needle-like growths. Furthermore, continued growth of the needles occurred until they almost completely encompassed the crystal surface when carbon deposition occurred. A grazing incidence X-ray analysis of such a surface, before the formation of free carbon, revealed only the presence of cementite (Fe_3C). However, when a crystal surface previously reacted to form the needle-like material was treated for 20 hr in a H_2 atmosphere at 550°C, the X-ray pattern remained unchanged. Despite this the crystal had assumed a greyish cast suggesting that some component which could not be identified from the X-ray data had been reduced.

This particular study is also significant in that by utilizing single crystal spheres the authors were able to correlate catalytic activity with differing atomic arrangements. They determined the following descending series for the rate of carbon growth on the various planes, minor faces > 211, 311 .... > 221, 331 .... > 210, 310 .... > 111 and 110 > 100. It is emphasized that these planes refer to an Fe lattice.

At the time of writing this paper, Ruston *et al.* (*17*) published a study of the solid reaction products resulting from the breakdown of CO over Fe single crystals in which they concluded that both Fe and Fe_7C_3 were active catalysts for this reaction. However, as pointed out below, the X-ray powder patterns used to identify this carbide are open to other interpretations.

Experimental Methods

Materials

The present study of the disproportionation of CO over Fe and 3.5% Si–Fe single crystals was initiated in an attempt to differentiate between the above mentioned possible catalytic species. The original reasons for employing both Fe and Si–Fe were threefold:

(i) It has been suggested that there is a resurgence in the rate of CO disproportionation over Fe above ca. 800°C, which could possibly result from the greater solubility of carbon in the BCC than in the FCC Fe lattice. This α to γ transition, which occurs at 723°C for the Fe–Fe_3C system, is completely repressed by the addition of 3.5% Si.

(ii) Although it is relatively easy to carbide Fe above 200°C, 3.5% Si–Fe is carbided only with considerable difficulty by reaction in H_2–heptane mixtures far in excess of the above temperature (*21*). This could clearly be advantageous in determining the role of carbides in this reaction.

(iii) In contrast to Fe crystals, it is not too difficult to arrange for arrays of pure edge and pure screw dislocations to intersect different faces of the same Si–Fe single crystal. By suitable heat treatment the edge dislocations become polygonized forming linear arrays which are sessile under the conditions utilized for the disproportionation reaction. It is important to know if such dislocations act as active sites for the nucleation of reaction products at the Fe surface, or whether perhaps they promote a solid-state reaction between C and Fe. It is well known that the dislocations in both Fe and Si–Fe crystals are preferentially decorated by C atoms (*21*).

Single crystal beams of both Fe and 3.5% Si–Fe, having the dimensions 12 × 2.5 × 1.25 mm, were cut from larger crystals employing a jewelers saw. After being mechanically polished through 4/0 silicon carbide paper a back reflection Laue X-ray diffraction technique showed the beams to be within 3° of the orientation depicted in Fig. 1. According to Kehrer and Leidheiser (*20*) (see above) the (211) face provides

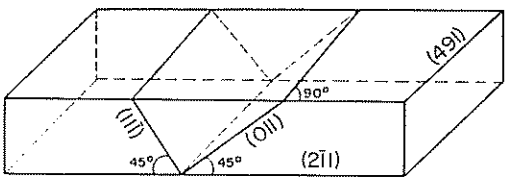

Fig. 1. Schematic representation of the crystal orientation employed.

one of the most catalytically active surfaces. When required, dislocation arrays were introduced by four-point bending using an Instron Testing Machine. Prior to reaction the beams were electropolished in a Morris bath (*22*) and then annealed in dry H_2 at 650°C for several hours.

Research grade CO (Matheson Company, Inc., having the following main impurities, $CO_2 < 70$ ppm; $O_2 < 3$ ppm; $N_2 < 100$ ppm) was used in all the static experiments involving this gas; whereas, for the kinetic experiments cylinder CO (99.8% purity) was employed. In other experiments a mixture of CO–9.4% H_2 from a cylinder (Matheson Company, Inc., main impurities being 0.018% O_2 and 0.14% CO_2) was employed. The cylinder gases were in some instances purified by passing through an Ascarite tower to remove CO_2, a Drierite tower to remove H_2O, and a furnace at 250°C to decompose any Fe carbonyls that might be present. The partial pressure of the water vapor present in the system could be controlled by varying the refrigerent in a cold trap.

Maghemite (γ-Fe_2O_3) powder was prepared by the method of David and Welch (*23*). The fraction passing through a 200, but not a 325, mesh sieve was used for experimentation. An X-ray diffraction analysis of the powder showed that it contained a small percentage of hematite (α-Fe_2O_3).

Method

Static experiments were carried out in a double-walled quartz reaction vessel which could be evacuated to a pressure of 10^{-7} Torr, as recorded on an ionization gauge. A reaction temperature of 550°C, controlled to ±1°C was employed in most experiments, and unless otherwise stated the gas pressure was 1 atm. Kinetic data were obtained with a Cahn RG electrobalance which was incorporated into a conventional high vacuum system.

The crystal surfaces and reaction products were examined at various stages of the reaction by optical microscopy (Reichert Zetopan), transmission electron microscopy, transmission and reflection electron diffraction with the projector lens turned off (Hitachi HU-11), and X-ray powder diffraction. Either Au or Pt was used as an internal standard to determine the relevant diffraction constant of the microscope.

Results

Formation of the Catalytic Species in a CO–9.4% H_2 Mixture

On Fe surfaces. The photomicrograph shown in Fig. 2 depicts the (211) surface of an Fe crystal after 30-min reaction in a CO–9.4% H_2 mixture (introduced into the reaction chamber from the cylinder without further purification) at 550°C. The needle-like platelets evident here are approximately 100 μ long, 10 μ wide, and 1 μ thick. Under these particular conditions growth of the platelets was observed to continue for periods up to 3 hr before either a carbide, or carbon was nucleated. Once initiated the disproportionation reaction then led rapidly to the formation of a complete product layer which consisted of both carbides and carbon (see below). Microscopic examination of the Fe crystal, after removal of the products by mechanical and electropolishing techniques, did not reveal any evidence to indicate the formation of carbides within the bulk of the crystal.

Examination of the crystal surface by reflection electron diffraction prior to carbon formation (the presence of carbon was sought by electron microprobe analysis) yielded the diffraction pattern shown in Fig. 3a. In this instance, the diffraction constant of the microscope was determined from reflections arising from a Au film laid down on one half of the surface under investigation. From the orderly array of diffraction spots in Fig. 3a, it is concluded that the initial reaction product was single crystal in nature and had grown either epitaxially or topotactically on the Fe single crystal substrate. On indexing the pattern the reflections were shown to be consistent with those expected from the (031) reciprocal lattice net of γ-Fe_2O_3, (see Fig. 3b). The faint extraneous spots in this pattern could have arisen both from diffraction in a different underlying oxide lattice and by double diffraction. The weak rings corre-

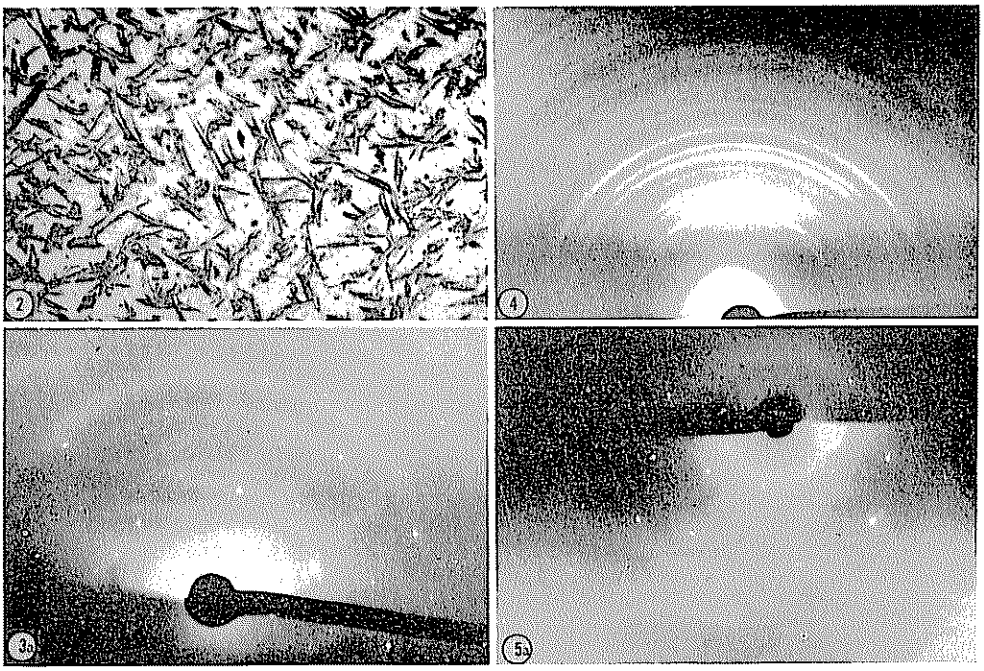

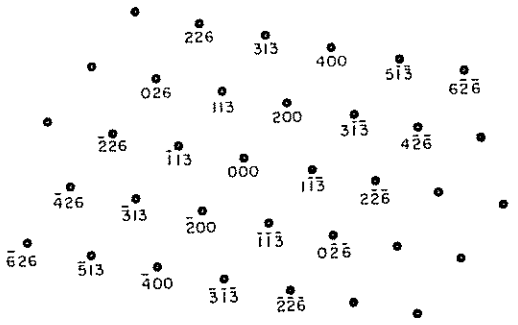

Fig. 3b

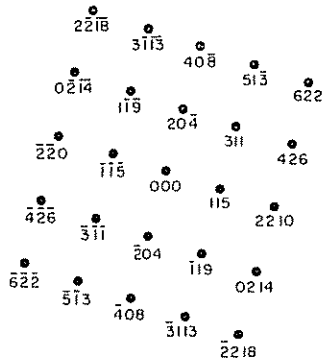

Fig. 5b

Fig. 2. Acicular plates of γ-Fe_2O_3 formed on the (211) face of an Fe single crystal after approximately 30-min reaction in a CO/9.4% H_2 mixture at 550°C. (×150).

Fig. 3a. Reflection electron diffraction pattern obtained from the surface depicted in Fig. 2. (b) Reciprocal lattice net in the γ-Fe_2O_3 structure corresponding to the diffraction pattern shown in Fig. 3a.

Fig. 4. Reflection electron diffraction pattern from the (211) surface of an Fe single crystal reacted for 30 min in a further purified CO/9.4% H_2 mixture.

Fig. 5a. Reflection electron diffraction pattern from the (211) surface of a 3.5% Si–Fe single crystal reacted for approximately 30 min in a CO/9.4% H_2 mixture at 550°C. (b). Reciprocal lattice net in the γ-Fe_2O_3 structure corresponding to the diffraction pattern shown in Fig. 5a.

spond to reflections from the Au lattice, formed by the electron beam overlapping both the oxide and Au films present on the crystal surface.

It is noted that, because of the similarity of the two crystal lattices, it is sometimes difficult to unequivocally differentiate between the oxides Fe_3O_4 and γ-Fe_2O_3 by a diffraction analysis. In the above case, the identification of γ-Fe_2O_3 is based on the

observation of reflections at the lower θ values which are forbidden by the symmetry of the Fe_3O_4 lattice.

When the CO–9.4% H_2 mixture was further purified (as described above) prior to reaction with the Fe crystal, the character of the oxide formed was markedly different. The oxide film grew more rapidly, the crystal surface being completely covered in the first few minutes of reaction, and it sometimes attained a thickness of ca. 20 μ. However, the induction period for the initiation of carbon growth, as measured from the time of admission of the gas mixture to the reaction chamber, was not substantially different.

A typical reflection electron diffraction pattern obtained from the outer surface of this oxide is shown in Fig. 4. This clearly demonstrates that the grain size of the oxide is very small. The measured interplanar spacings from this pattern, together with the ASTM X-ray diffraction data for Fe_3O_4, γ-Fe_2O_3, and α-Fe_2O_3, are listed in Table 2.

TABLE 2
DIFFRACTION DATA FOR OXIDE FILM FORMED ON Fe IN A PURIFIED CO/H_2 MIXTURE AT 550°C

Observed d-spacings (Å)	ASTM d-spacings (Å)		
	γ-Fe_2O_3	α-Fe_2O_3	Fe_3O_4
3.83^{vw}	3.86^{12}		
3.22^{m}	3.22^{25}		
3.09^{vw}	3.08^{2}		
2.92^{m}	2.95^{100}		2.97^{70}
2.69^{s}		2.69^{100}	
2.62^{vw}	2.64^{25}		
2.40^{w}	2.41^{8} [a]		2.42^{10} [a]
2.29^{m}	2.32^{8} [a]	2.29^{2}	
2.22^{vw}	2.21^{4} [a]	2.20^{30}	2.10^{70} [a]
2.01^{m}	2.01^{100}	2.07^{2} [a]	2.01^{70}
1.85^{m}	1.86^{2} [a]	1.84^{10}	
1.73^{m}	1.70^{100} [a]	1.69^{60}	1.71^{60}
1.62^{m}	1.61^{100}	1.63^{14}	1.61^{85}
1.58^{vw}	1.59^{2}	1.60^{16}	
1.43^{m}	1.43^{15}	1.45^{35}	
1.37^{m}	1.35^{20}	1.35^{4}	
1.33^{m}	1.32^{100}	1.31^{20}	1.33^{20} [a]
1.21^{m}	1.21^{50}	1.21^{4}	1.21^{30} [a]
1.16^{m}	1.14^{5}	1.14^{12}	

[a] Identification of these reflections is dubious.

It is apparent from the intensity of the individual rings, particularly the one at 2.69 Å, that the principal outer oxide phase formed under these conditions was α-Fe_2O_3. [Note, this does not imply that α-Fe_2O_3 grows more rapidly than the cubic oxide phases, such an assumption would be incorrect (*24*)]. The fairly strong reflection corresponding to an interplanar spacing of 3.2 Å was noted on a number of occasions and its origin remains somewhat of a mystery. However, the reflection electron diffraction pattern from an Fe crystal reacted in O_2 under conditions known to form α-Fe_2O_3 (*24*) gave a pattern similar to that in Fig. 4 and also contained the reflection at 3.2 Å. Maghemite, present as a small percentage of the total oxide, is identified from the very weak reflections observed at the lower θ values. It is possible that the medium intensity reflections corresponding to interplanar spacings of 2.92, 2.01, and 1.61 Å, respectively, arise in part from a small quantity of Fe_3O_4 residing in the oxide surface layer.

In order to determine the thermal stability of γ-Fe_2O_3 above 550°C a series of experiments were carried out, employing a CO–9.4% H_2 mixture (without further purification), in which the temperature was increased successively by increments of 25°C. A freshly electropolished crystal was employed for each experiment. Electron diffraction analysis of the films so formed showed that as the temperature was increased α-Fe_2O_3 rapidly became the dominant oxide phase. The temperature corresponding to the minimum detectable amount of γ-Fe_2O_3 was 625°C. The diffraction pattern from the film grown at this temperature was very similar to that presented in Fig. 4.

On 3.5% Si–Fe. The substitution of 3.5% Si–Fe for Fe yielded results similar to those described in the previous section. Figure 5a represents a reflection electron diffraction pattern obtained from the oxide formed on a Si–Fe crystal reacted in CO–9.4% H_2 (without further purification) at 550°C prior to carbide, or carbon nucleation. This pattern corresponds to a reciprocal lattice plane in the γ-Fe_2O_3 lattice (see Fig. 5b).

TABLE 3
SUMMARY OF DIFFRACTION RESULTS ON SINGLE CRYSTALS

Starting material	Gaseous atmosphere at 1 atm pressure	Temp (°C)	Stage at which solid products were studied	Initial oxide formed at crystal surface as determined by electron diffraction	Products as identified By X-ray powder diffraction
Fe (211)/(491)	CO–9.4% H_2 direct from tank	550	Induction period prior to carbon growth	Single crystal γ-Fe_2O_3	
	CO–9.4% H_2 direct from tank	550	Conclusion of reaction		Graphite, Fe_3C
Si–Fe (211)/(491)	CO–9.4% H_2 direct from tank	550	Induction period prior to carbon growth	Single crystal γ-Fe_2O_3	
	CO–9.4% H_2 direct from tank	550	Conclusion of reaction		Graphite, Fe_3C
Fe (211)/(491)	CO + H_2O vapor $\frac{P_{H_2O}}{P_{CO}} = 6.2 \times 10^{-3}$	550	Induction period prior to carbon growth	Polycrystalline γ-Fe_2O_3 or Fe_3O_4	
	Purified CO–9.4% H_2	550	Induction period prior to carbon growth	α-Fe_2O_3 + small amount of γ-Fe_2O_3	
	Purified CO–9.4% H_2	550	Conclusion of reaction		Graphite, Fe_3C
	Research grade CO	550	After 2 days		Fe, Fe_3C, Fe_2C No graphite
Si–Fe (211)/(491)	CO–9.4% H_2 + H_2O vapor $\frac{P_{H_2O}}{P_{CO/H_2}} = 6.2 \times 10^{-3}$	550	Induction period prior to carbon growth	Single crystal γ-Fe_2O_3	
	Purified CO–9.4% H_2	550	Induction period prior to carbon growth	α-Fe_2O_3 + small amount of γ-Fe_2O_3	
γ-Fe_2O_3	Purified CO	550	At approximately the end of the reduction stage		Fe, Fe_3C, Fe_2C, FeO; very weak graphite reflections
	CO + H_2O vapor $\frac{P_{H_2O}}{P_{CO}} = 7.73 \times 10^{-4}$	550	At approximately the end of the reduction stage		Fe, Fe_3C, Fe_2C, FeO; very weak graphite reflections
	Purified CO	550	After 20% reaction		Graphite, Fe_3C, Fe_2C; very weak Fe reflections; no FeO reflections
	Purified CO	550	Conclusion of reaction		Graphite and Fe_3C
	Research grade CO (8 cm)	550	After 2 days		Fe, Fe_3C, graphite

Again, when the Si–Fe was reacted in CO–9.4% H_2 which had been purified, the same oxide phases resulted that were previously found in the case of Fe; namely, α-Fe_2O_3, a very much smaller percentage of γ-Fe_2O_3, and perhaps Fe_3O_4. However, under both sets of experimental conditions the induction period for carbon growth was now about half that noted for pure Fe.

In an attempt to establish the influence of lattice defects on the reaction, a plastically deformed Si–Fe crystal containing well-defined rows of edge and screw dislocations which intersected the (211) and (491) crystal faces, respectively, was reacted in the gas mixture of 550°C. Microscopic examination of the crystal surfaces at various stages of the reaction failed to furnish evidence for the preferential nucleation of either oxide or carbonaceous products at the dislocation sites.

Finally, a summary of the results discussed above concerning the outer oxide phase formed both on Fe and Si–Fe single crystals reacted in CO–9.4% H_2 taken from a cylinder is given in Table 3. In addition, Table 3 includes a brief resumé of an X-ray powder diffraction study designed to elucidate the nature of the solid carbonaceous products of the reaction.

Formation of the Catalytic Species in CO

An Fe single crystal was reacted at 550°C in CO (research grade) at a pressure of 160 Torr. Almost immediately after admitting the gas, a bluish colored film appeared at the crystal surface. After a reaction time of 10 min, the crystal was removed from the system and examined by reflection electron diffraction. Analysis of the diffraction pattern showed that the outer surface consisted predominately of α-Fe_2O_3.

In a similar experiment, an Fe crystal was allowed to react for 93 hr in CO when a grey layer of reaction products formed. The latter was carefully stripped from the surface of the Fe crystal and examined by X-ray powder diffraction. The resulting pattern indicated the presence of Fe_2C, Fe_3C, and Fe. However, it is quite possible that the latter had been inadvertently re-

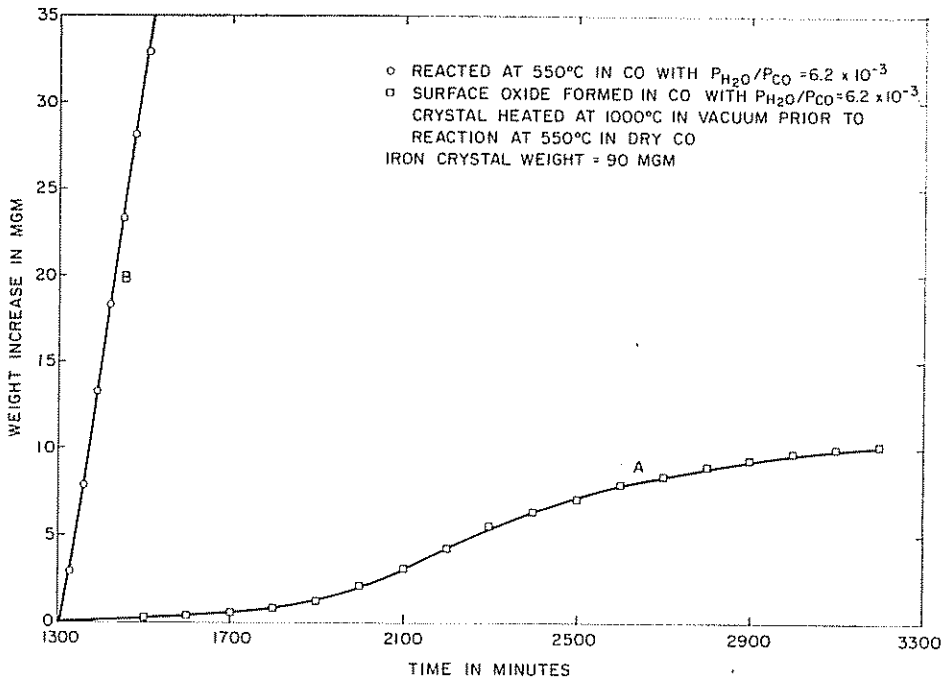

FIG. 6. Effect of water vapor on the rate of carbon formation from CO disproportionated over an Fe single crystal.

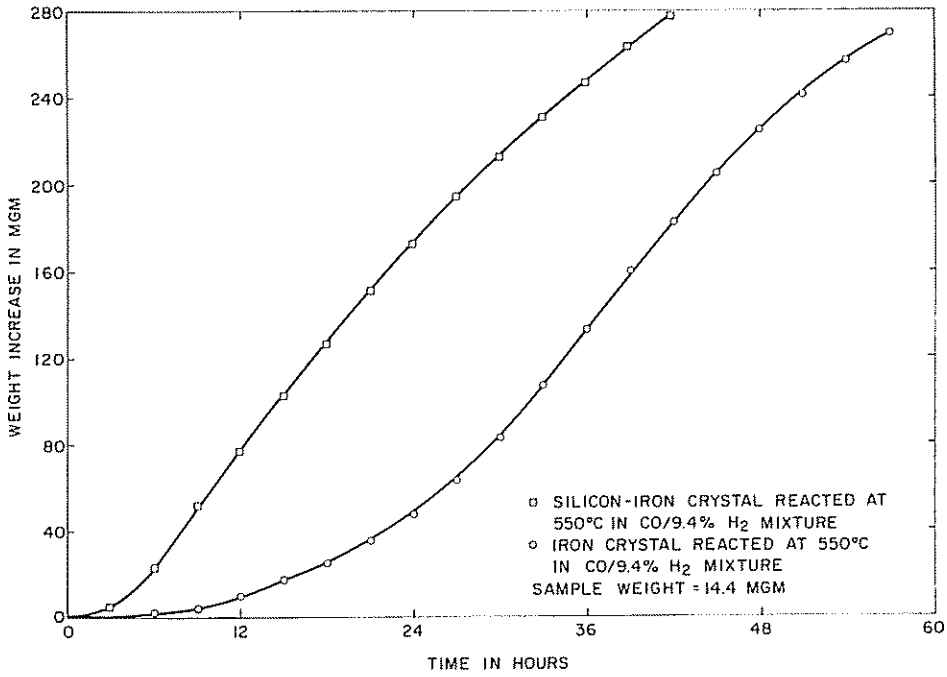

FIG. 7. Rates of carbon formation over Fe and 3.5% Si–Fe.

moved from the crystal surface. In another experiment an Fe crystal was first reacted for 100 hr in CO (160 Torr) and then H_2 (35 Torr) was admitted to the reaction chamber. Within 1 hr carbon began to form at the crystal surface.

In view of the above results, the effect of small amounts of water vapor on the mode of reaction was investigated. The reflection electron diffraction patterns obtained from the surface of an Fe crystal reacted for 15 min in CO with a P_{H_2O}/P_{CO} ratio of 6.2×10^{-3} indicated that the outer oxide scale corresponded to either Fe_3O_4 or γ-Fe_2O_3. Unfortunately, for reasons cited earlier, it was not possible in this instance to differentiate between these two oxide phases. Essentially the same results were found when a Si–Fe crystal was substituted for Fe.

The data from this section is also summarized in Table 3.

Microbalance Studies

Effect of water vapor on the reaction rate. It was considered that a rigorous kinetic study was not justified at this time because of the complicated reaction scheme thought necessary to adequately describe the disproportionation reaction. Instead, specific experiments were designed to compliment the results obtained by microscopic and diffraction techniques.

A measure of the effect that small amounts of water vapor have on the rate of CO disproportionation over single crystal Fe is recorded in Fig. 6. An Fe crystal was reacted at 550°C in CO (taken from a cylinder) for which $P_{H_2O}/P_{CO} = 6.2 \times 10^{-3}$. The reaction was eventually discontinued after 1500 min when 37 mg of carbon had formed. An almost identical crystal was then reacted at 550°C in a gas mixture having the same P_{H_2O}/P_{CO} ratio for 10 min, a period sufficient to produce a film of the inverse spinel type oxide. The system was then evacuated and the crystal was heated to 1000°C. This temperature was maintained for 12 hr to ensure the complete removal of the H_2O associated with the oxide lattice (*25*). The furnace was subsequently cooled to 550°C and CO (taken from a cylinder and further purified) was admitted. This experiment was

taken to completion when after 2000 min the observed increase in weight was 10 mg. In both experiments the induction period was ca. 1300 min.

Comparison of the catalytic activity of Fe and Si–Fe crystals. Crystals of both Fe and Si–Fe, having the orientation schematically represented in Fig. 1 and possessing similar surface areas, were successively reacted at 550°C on the microbalance in a CO–9.4% H_2 mixture. In each instance, it was necessary to prematurely terminate the reaction because the extent of carbon formation was such that the latter eventually fell from the quartz container. Some notion of the mechanical strength of the material produced is given by the fact that on some occasions the latter extended as much as 2 cm from the individual crystal faces before breaking off. For both Fe and Si–Fe the curves obtained, see Fig. 7 for typical examples, were sigmoidal. However, the point of inflection for the curve corresponding to Si–Fe occurred after only 8 hr, whereas for Fe the inflection point was not apparent until a reaction time of 36 hr. It is expected that the total carbon yield would be approximately the same for both crystal types.

Powdered γ-Fe_2O_3. In an attempt to relate this study to previous investigations in which powdered catalysts were employed, a limited number of experiments were carried out using γ-Fe_2O_3 powder as the starting material. All the experiments involving γ-Fe_2O_3 were conducted at 550°C and a total gas pressure of 1 atm. Before admitting the gas, the sample was brought to the reaction temperature and the microbalance read out allowed to stabilize.

Figure 8 depicts a typical cross section of the data compiled in this manner. Curve I represents the reaction of γ-Fe_2O_3 with a CO–water vapor mixture for which the P_{H_2O}/P_{CO} ratio was 7.73×10^{-4}. The initial reduction of the oxide caused the sample weight to decrease during the first 10 min of reaction, after which time the curve passed through a minimum and a linear rate of carbon formation of 5.53×10^{-4} g/min was established. By lowering the partial pressure of water vapor to a value

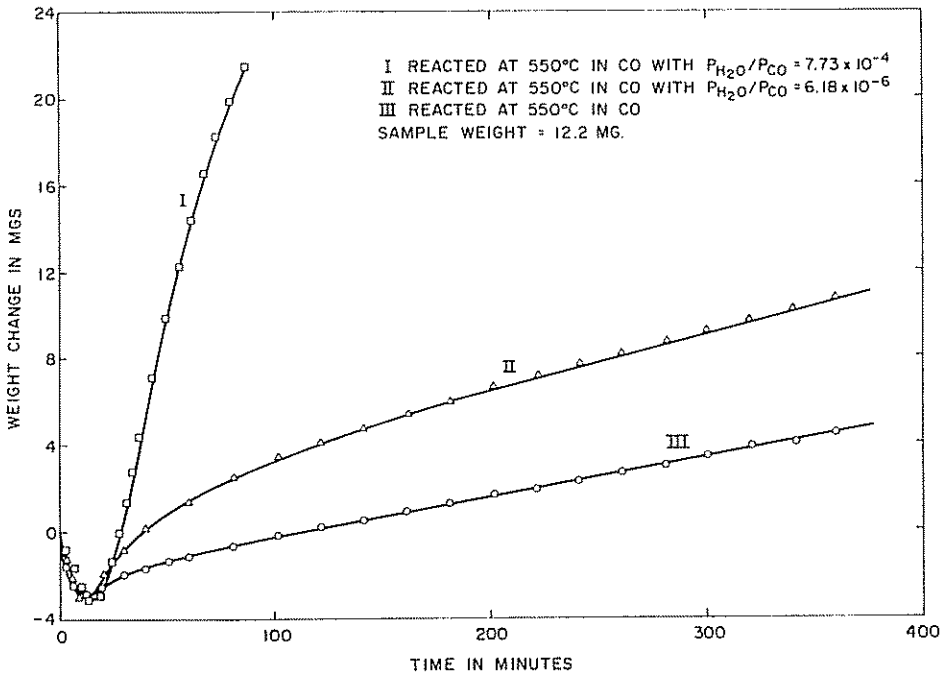

FIG. 8. Effect of water vapor on the rate of carbon formation from the disproportionation of CO over γ-Fe_2O_3 powder.

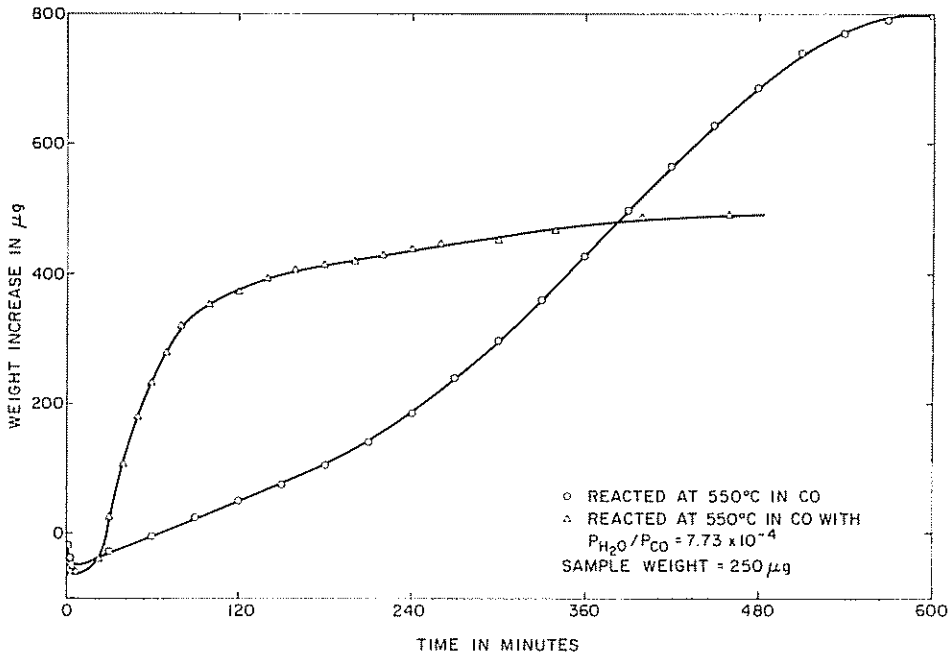

FIG. 9. Deleterious effect of water vapor on the total yield of carbon formed over γ-Fe_2O_3 powder.

concomitant with a P_{H_2O}/P_{CO} ratio of 6.18 $\times 10^{-6}$, the linear rate of reaction was reduced by more than an order of magnitude to 2.57×10^{-5} g/min, see Curve II. Curve III, representing the weight change noted when CO (purified) was employed, is included in Fig. 8 for comparative purposes.

The possible influence of water vapor on the products of the disproportionation reaction was determined by performing an analogous set of experiments to those typified in Curves I and III. When the reaction was prematurely terminated at a stage corresponding to the minimum in the weight change curve, an X-ray diffraction analysis showed that for both sets of experimental conditions the products were Fe, Fe_2C, Fe_3C, wustite (FeO), and a trace amount of graphite. After the reactions had gone approximately 20% toward completion, analysis of the products showed that the graphite, Fe_2C and Fe_3C reflections were strong, whereas the Fe reflections were very weak and the FeO reflections had completely disappeared. At the conclusion of the reaction graphite and Fe_3C were the only products identified. The results are summarized in Table 3.

The deleterious effect of water vapor on the total yield of carbon produced in the catalyzed disproportionation reaction is demonstrated by Fig. 9. When CO having a P_{H_2O}/P_{CO} ratio of 7.73×10^{-4} was employed, a faster linear rate was realized but the final carbon yield was only 66% of that noted for dry CO.

Optical and Electron Microscope Investigation of the Carbonaceous Products

Examination under the optical microscope showed that the final products of the disproportionation reaction over both Fe and Si–Fe crystals consisted of a platelet material and two distinct types of fibrous material. The former was easily identified as small deformed graphite crystals. Some of the graphite fibers, which previous authors (*26*, *27*) have shown to be so characteristic of this reaction, are up to 0.3 mm in length and even longer fibers probably exist which are interwoven in the rigid mass comprising the bulk of the reaction products. The second type of fibrous material, which is present to a lesser extent than the graphite fibers described above, is represented in Fig. 10. These fibers are

considerably coarser than the others and are typically found in discrete, well-defined bundles.

More detailed information concerning the individual components of the carbonaceous product was obtained in an electron microscope study. For this study, sample products were taken after the reaction had proceeded approximately 20% toward completion. The transmission electron micrograph, Fig. 11, illustrates the three typical conformations, namely helical, spiral, and straight, taken up by the graphite fibers. The diameter of the fibers, with the notable exception of those displaying a helical conformation, have a diameter of about 0.5 μ.

Figure 12 is particularly significant because it clearly shows that the graphite fibers emanate from relatively large platelets of an intermediate product of the reaction. One of the selected area diffraction patterns obtained from the tip of this source for fiber growth is presented in Fig. 13, and a complete listing of all the reflections obtained from this material is given in Table 4. From this analysis it was concluded that the intermediate product in question was Fe_3C. In a similar manner, the presence of this carbide was also detected in the fibrous material shown in Fig. 12.

Further careful searching of the sample in the electron microscope revealed another piece of an intermediate product (see Fig. 14) which was much more suitable for transmission electron diffraction. All the patterns obtained from this sample were complicated by the fact that the latter consisted of an agglomerate of several

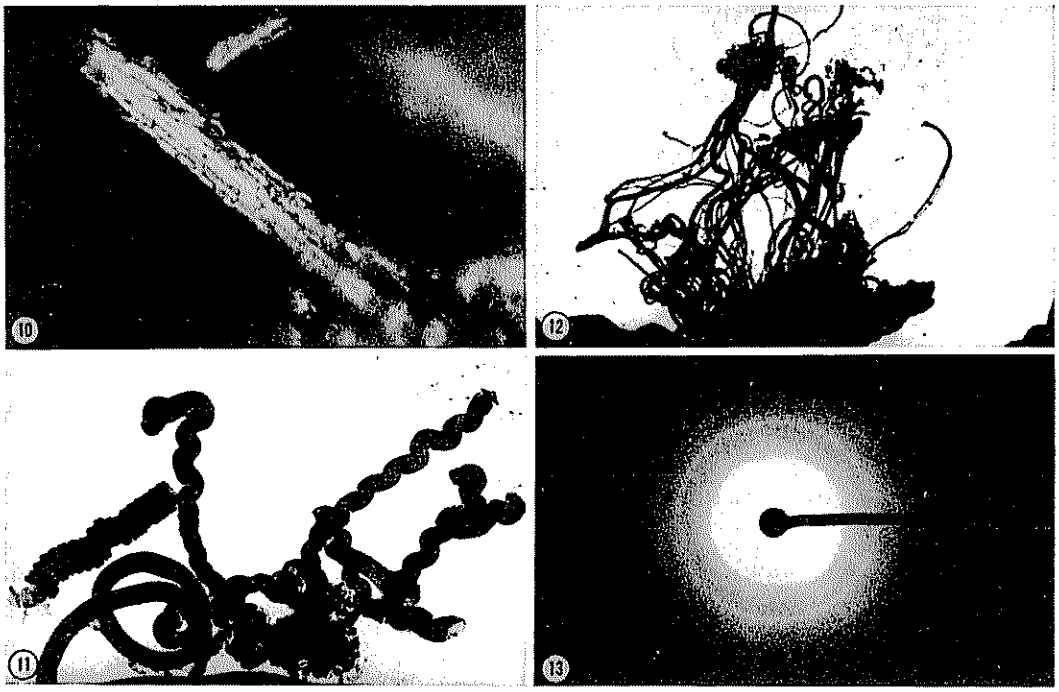

FIG. 10. Bunch of relatively thick fibers observed in the carbonaceous reaction products formed on an Fe crystal. (×500).

FIG. 11. Transmission electron micrograph depicting the three typical conformations exhibited by the fibers constituting the bulk of the reaction products. (×24,000).

FIG. 12. Transmission electron micrograph showing a cluster of fibers emanating from an intermediate reaction product. (×24,000).

FIG. 13. Selected area diffraction pattern obtained from the tip of the intermediate product shown in Fig. 12.

TABLE 4
DIFFRACTION DATA CORRESPONDING TO THE PATTERN DEPICTED IN FIG. 13

Observed *d*-spacings (Å)	ASTM *d*-spacings (Å)	
	Fe_2C	Fe_3C
3.28	3.31^{30}	
2.69	2.64^{50}	
2.28	2.28^{60}	2.26^{25}
2.02	2.02^{50}	2.02^{60}
1.99	1.99^{50}	1.97^{55}
1.64	1.66^{30}	1.68^{15}
1.18	1.18^{20}	

platelets which apparently were not all of the same carbide phase. For instance, the pattern given in Fig. 15 was obtained from an area in which there were two overlapping platelets and consequently two single crystal patterns can be identified along with a number of satellite reflections arising from double diffraction. The pattern designated by circles yielded a set of interplanar spacings (see Table 5) which appears to correspond closely with those of the Fe_2C lattice as given by Jack (*28*). Despite this it was not possible to correlate this pattern with a reciprocal lattice plane in the Fe_2C structure. The interplanar spacings determined from the other pattern (which for convenience of identification has been marked out by a set of triangles) do not correspond to any listed spacings for an iron carbide, even when the appearance of what are normally considered as forbidden reflections is taken into account (see Table 5). As a result, it is suggested that both of these patterns arise from the presence of a series of carbides having compositions intermediate between Fe_2C and Fe_3C (*29*).

TABLE 5
DIFFRACTION DATA CORRESPONDING TO THE COMPOSITE SINGLE CRYSTAL PATTERN SHOWN IN FIG. 15

Observed *d*-spacings from (Å)		ASTM *d*-spacings (Å)	
△ Pattern	○ Pattern	Fe_2C	Fe_3C
	4.53	4.56[a]	
4.38			
4.17			
	3.87	3.86[a]	
3.66			
	3.52	3.56[a]	
2.65			
	2.56	2.50^{60}	2.54^{5}
	2.23	2.20^{70}	2.26^{25}
	2.07	2.08^{100}	2.05^{70}
	1.72	1.73^{50}	1.76^{15}

[a] Calculated spacings.

An interesting feature of the graphite fibers is that they sometimes contain diamond or hexagonal shaped particles of another material. In Fig. 12, two such particles are distinguishable approximately halfway along the length of the two immediately adjacent fibers located on the far right of the micrograph. It is noteworthy that an almost identical situation was found by Hofer *et al.* (*26*) in the carbon products formed during the disproportionation of CO over a Co catalyst.

The microstructural details of a graphite fiber containing one of these second-phase particles is more clearly resolved in the higher magnification transmission electron micrograph, Fig. 16. Typically the tiny individual graphite crystallites tend to be radially disposed about a hollow core which completely traverses the length of all the uncollapsed fibers. In every instance the second-phase particles were completely contained within the confines of the fiber in the manner illustrated in Fig. 16. The selected area electron diffraction pattern obtained from this particular particle is given in Fig. 17a. This was one of the very few patterns taken which was sufficiently complete to allow the identification of the second phase as Fe_3C. The corresponding reciprocal lattice net is presented in Fig. 17b. The presence of reflections forbidden by the symmetry of the orthorhombic cell of Fe_3C result from the overlap of diffraction spikes centered on adjacent reciprocal lattice planes which are displaced along the *c* axis. Such diffraction spikes are normally a feature of very thin transmission specimens.

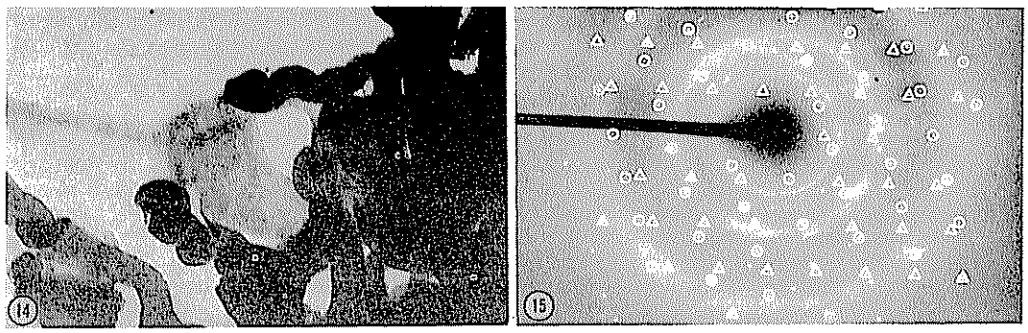

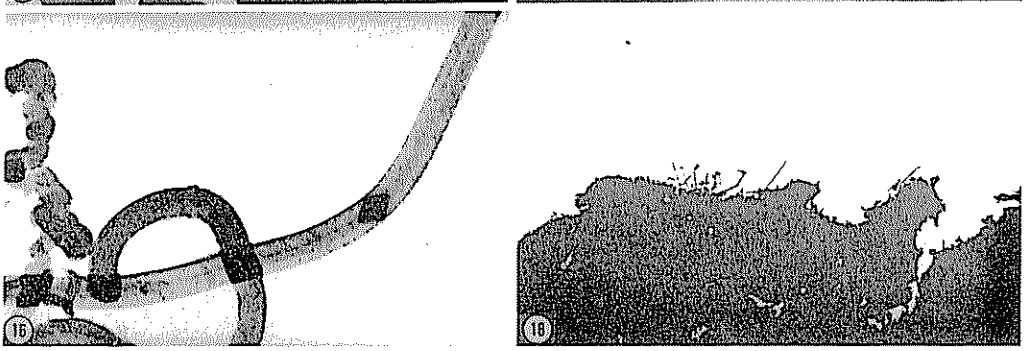

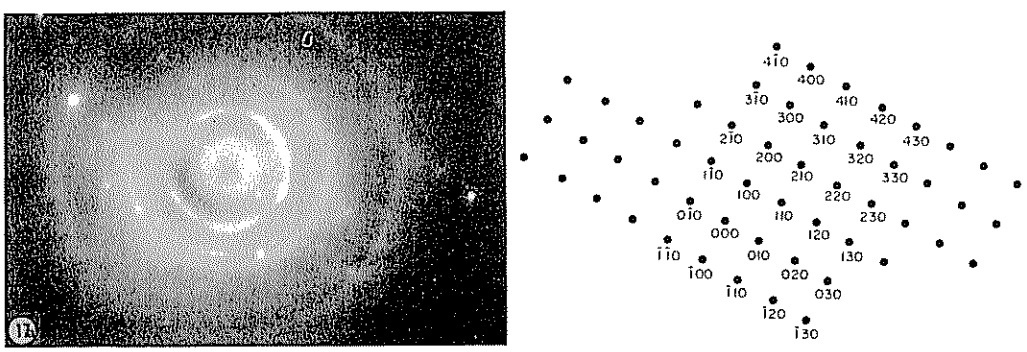

FIG. 17b

FIG. 14. Transmission electron micrograph showing plate-like material formed during product growth. (×55,000).

FIG. 15. Selected area diffraction pattern obtained from the plate-like material shown in Fig. 14. This pattern is a composite of two single crystal patterns which are identified by Δ's and O's, respectively, for the sake of clarity.

FIG. 16. Transmission electron micrograph showing a second-phase particle residing within a graphite fiber. (×55,000).

FIG. 17a. Selected area diffraction pattern obtained from the second-phase particle shown in Fig. 16. (b). Combination of the reciprocal lattice nets in the cementite structure corresponding to the diffraction pattern shown in Fig. 17a.

FIG. 18. Transmission electron micrograph of carbide whiskers protruding from a graphite crystal grown from an Fe–C solution. (Observation in the optical microscope indicated that the maximum length of the whiskers was 0.5 mm.)

Formation of Carbide Whiskers in Fe–C Melts

It is pertinent to the establishment of a mechanism responsible for the formation of the graphite fibers to consider briefly here some results generated during attempts to grow large graphite single crystals in these laboratories by passing a thin zone of molten Fe through a rod of polycrystalline graphite (*30*). Figure 18 represents an electron micrograph of a portion of a thin crystal grown in this manner which had been mounted on the reflection stage of the microscope. With the crystal in this orientation, it was possible to take a set of transmission electron diffraction patterns with the incident beam engulfing a number

FIG. 19. Transmission electron diffraction pattern from a group of the whiskers shown in Fig. 18.

of the whiskers which are seen to protrude from the crystal surface. The length of some of these whiskers, as determined under the optical microscope, was in the region of 0.5 mm. An example of the type of pattern obtained, which corresponds to diffraction from an Fe_3C lattice, is given in Fig. 19. In this particular instance the diffraction constant of the microscope was determined by means of a Pt film deposited on the upper surface of the reflection stage.

DISCUSSION

The initial product of the reaction of both Fe and Si–Fe single crystals with a CO–9.4% H_2 mixture, taken directly from a cylinder, was an oxide layer. The outer oxide scale was identified by reflection electron diffraction as either γ-Fe_2O_3 or, alternatively, a solid solution $Fe_{3-Z}O_4$, where $1/3 > Z > 0$, which is thought to possess a very similar crystal structure (*31*). This oxide layer is in all probability extremely thin, and it should be noted in this connection that in reflection electron diffraction the electron beam is thought to penetrate the surface under study by only 20–40 Å (*32*). Free energy diagrams show that an oxygen partial pressure of 10^{-15} atm is sufficient to oxidize Fe to Fe_2O_3 at 550°C. Such oxygen pressures are present even when employing research grade CO.

Copious amounts of carbon were produced under these conditions indicating that the γ-Fe_2O_3 type lattice acts as an excellent catalytic species for the disproportionation of CO. Although the γ-Fe_2O_3 lattice is tetragonal it closely approximates to a defective inverse spinel structure which would contain $2\frac{2}{3}$ cation vacancies per unit cell. The molecular formula may be represented by $Fe\square_{1/3}\ Fe_{5/3}O_4$, where $\square$ signifies a cation vacancy. The presence of these defect sites is extremely important to the function of the oxide as a catalyst, because they provide a pathway for the diffusion of the cations through the oxide layer to the gas–solid interface. It is proposed here that these ions then facilitate the chemisorption and subsequent rupture of the CO molecule on the oxide surface.

When a procedure was adopted to further purify the CO–9.4% H_2 mixture prior to reaction by lowering the H_2O, CO_2, and possibly carbonyl impurity concentrations (*33*) an oxide layer formed more rapidly on the Fe surface. The outer scale in this instance was found to be α-Fe_2O_3, which suggests that the oxide subscales must have been responsible for the enhanced growth rate. This is in accord with the findings of Boggs *et al.* (*24*) that the rate of oxidation, due to the growth of an Fe_3O_4 scale, is proportional to the inverse of the oxygen potential in the reaction system. The same result was also found when research grade CO was substituted for the gas mixture. An experiment was then performed in which a small addition of H_2O vapor was made to the research grade CO, the P_{H_2O}/P_{CO} ratio being 6.2×10^{-3}. Unfortunately, from the ensuing reflection electron diffraction

analysis, it was not possible to decide unequivocally whether the outer oxide scale was Fe_3O_4 or γ-Fe_2O_3. However, in view of the previously stated results, it is tentatively assumed that the oxide was γ-Fe_2O_3.

The sequence of experiments described so far strongly suggest that water vapor plays the extremely important role in the catalyzed reaction of stabilizing the γ- as opposed to the α-modification of Fe_2O_3. This result is supported by a study (*25*) in which it was established that for the topotactic transformation of Fe_3O_4 to γ-Fe_2O_3 to occur during oxidation, it is necessary for the Fe_3O_4 lattice to contain a high density of lattice defects. In the disproportionation experiments this condition would be satisfied when water vapor was present in the oxidizing atmosphere, because it is believed that this leads to the substitution of highly mobile protons for the Fe cations in the oxide lattice (*25*).

The formation of γ-Fe_2O_3 at 550°C is in apparent contradiction to the observation (*34*) that the phase transformation γ-$Fe_2O_3 \rightarrow \alpha$-$Fe_2O_3$ has a significant rate at temperatures in excess of 400°C. However, Takei and Chiba (*35*) have recently described a procedure for the epitaxial growth of thin γ-Fe_2O_3 films in the temperature range 650–700°C by vapor phase deposition on to a (100) face of an MgO single crystal. They propose that the stability of the γ-Fe_2O_3 lattice results from the very close relationship existing between the atomic arrangement of the oxygen ions at the substrate surface and those in the (100) plane of γ-Fe_2O_3. If this argument is valid, it is then quite possible that in the present study the γ-Fe_2O_3 is stabilized by the underlying Fe_3O_4 lattice.

A set of experiments have been described which were designed to determine the thermal stability of γ-Fe_2O_3 films formed during the disproportionation of CO over Fe. Although α-Fe_2O_3 was not found in the oxide surface at a reaction temperature of 550°C, when the latter was raised to 625°C only a barely detectable amount of γ-Fe_2O_3 remained with α-Fe_2O_3 being the main component of the film. For the following reason, it is considered somewhat more than coincidental that in this same temperature range the rate of disproportionation of CO passes through a maximum and then falls quickly to a relatively low value. Hematite has a rhombohedral lattice which does not contain the cation vacancies associated earlier with the γ-Fe_2O_3 lattice. Therefore, the presence of even a very thin outer scale of α-Fe_2O_3 would impede the diffusion of the cations to sites where they could influence the dissociation of the CO molecule. Consequently, it is possible to predict the observed decrease in reaction rate at ca. 600°C on a reaction scheme which assumes the oxide γ-Fe_2O_3 to be the active catalytic species. It has been tacitly assumed throughout this text that an individual Fe particle will behave in a very similar manner to the single crystal material employed for most of this study.

It is pertinent at this juncture to note that Olmer (*12*) found that by the addition of MgO powder to Fe, also in a powdered form, both the maximum rate of reaction and the temperature at which it occurred were increased. Indeed the reaction rate he observed at 750°C was approximately equal to the maximum rate in the absence of MgO. It was supposed that the MgO influenced the reaction merely by limiting the particle size during sintering of the Fe. However, in terms of the present theory it seems probable that the MgO could also have modified the nature of the catalyst chemically. Provided it can be assumed that MgO is able to diffuse into the oxide, perhaps to a depth of ~100 Å, a thin scale of the spinel structure corresponding to $MgFe_2O_4$ would displace the α-Fe_2O_3 scale normally formed above 600°C. Under these circumstances the overall reaction rate at any temperature will depend only on the relative rates of the catalyzed forward and back reactions summarized in Eq. (1).

In consideration of the discussion so far presented, it appears reasonable to suppose that any *p*-type oxide of Fe, residing on an Fe substrate, which can be stabilized under the conditions pertaining to the disproportionation of CO will act as an effective catalyst. The studies of Taylor

(*2*), Trillat (*18*, *19*) and Kehrer and Leidheiser (*20*), respectively, also appear, at least in part, to substantiate this conclusion.

It seems likely that the needle-like crystals formed at the onset of reaction at 550°C on the single crystal Fe spheres employed by Kehrer and Leidheiser originally grew as an oxide, despite the fact that they were subsequently identified as Fe_3C. This is quite feasible provided sufficient CO had disproportionated before the reaction was terminated, so that the carbon formed could undergo a solid–solid interaction with the oxide to produce a carbidic phase. Evidence for believing that this type of reaction is of importance is discussed below. It is noted that Kehrer and Leidheiser were able to observe reflections from the Fe_3O_4 lattice in the X-ray patterns taken from crystal surfaces reacted at temperatures below 350°C where the rate of disproportionation is substantially slower.

The study of Ruston *et al.* (*17*) is particularly noteworthy here because despite the use of quite stringent experimental conditions, aimed at minimizing the concentration of foreign reactants, they nevertheless detected the formation of α-Fe_2O_3. Contrary to the viewpoint expressed in this text, the same authors concluded that the important catalytic species, which was again observed to form as an epitaxial deposit, was the carbide Fe_7C_3. However, it would appear that the X-ray diffraction powder patterns on which they base this premise can be interpreted equally as well in terms of the Fe_2C and α-Fe_2O_3 lattices.

If indeed an oxide phase acts as the catalytic species, the bulk properties of the Fe matrix should exert little influence on the disproportionation reaction. The following observations support this viewpoint.

(i) Neither the catalytic mode nor the reaction rate were modified by the intentional plastic deformation of a Si–Fe crystal prior to reaction.

(ii) By comparison of the reaction rates found over both Fe and Si–Fe crystals at 800°C, it was shown that the particular modification of the Fe lattice stable at this temperature was not of any great importance.

(iii) No evidence was found for any significant carburization of the Fe crystal during reaction which suggests that the mechanism for disproportionation put forward by Taylor is incorrect.

(iv) If chemisorption of CO on pure Fe is a major step in the disproportionation reaction then one would also expect Pt and Pd to be at least equally good catalysts since they chemisorb CO more strongly than Fe. The reason they are not is readily explained in terms of the present mechanism.

There is one apparent anomaly relating to the above arguments; namely, the addition of 3.5% Si to an Fe crystal results in both a shorter induction period for carbon growth and an increase in the initial reaction rate. To explain this phenomenon it appears necessary to assume that Si is, to some extent, incorporated in the oxide film. If this occurred, the Si would then be in a position where it could promote the graphitization of any intermediate carbide phase (*36*).

Some conception of the influence that relatively small amounts of water vapor exert on the disproportionation reaction at a temperature of 550°C can be gained by comparison of curves A and B, Fig. 6. It is suggested that there are two factors, both of which relate to the water vapor partial pressure in the reaction system, contributing to the very different results obtained in these two experiments. In the first instance, the reaction rate was probably appreciably depressed at the lower water vapor levels, see curve A, because of the formation of a thin outer scale of the relatively inactive oxide α-Fe_2O_3. Second, even after a reaction time of 93 hr an X-ray diffraction analysis indicated that the products of the reaction represented by curve A were principally the carbides Fe_2C and Fe_3C. Clearly then these species are not catalytically active in the disproportionation reaction. In contrast, graphite was a major product when the H_2O vapor level was raised to produce curve B. It is therefore concluded that water vapor is

instrumental in the breakdown of the carbides formed as intermediate reaction products.

This point is further substantiated by the curves shown in Fig. 8, which were obtained by reaction over a powdered catalyst. Haas *et al.* (*5*) have recently reported very similar findings which they suggested were a result of the formation of H_2 from the water gas shift reaction. In an earlier study Walker *et al.* (*4*) clearly describe the effect of varying the H_2 concentration in a CO–H_2 mixture on the reaction rate. However, it still remains difficult to rationalize the observation that the total yield of carbon is diminished by increasing the water vapor concentration. The initial weight loss recorded in the curves of Fig. 8 reflect the reduction of γ-Fe_2O_3, which was employed as the starting catalyst, to Fe and FeO. This implies that the formation of the γ-Fe_2O_3 scale on the Fe single crystals resulted from a kinetic balance of two competing reactions; namely (a) the oxidation of Fe by O_2, and (b) the reduction of the oxide by CO. It was not possible to detect in the products of reduction the presence of either an Fe_3O_4 or γ-Fe_2O_3 scale. However, in each instance the carbides Fe_2C and Fe_3C were present. This would suggest that before the reduction process had gone to completion sufficient carbon had formed to convert the outer oxide scales to these carbides. A similar explanation was given earlier in connection with the observations of Kehrer and Leidheiser (*20*).

The results presented in Fig. 17a and b provide further corroboration for believing that the formation of a carbide, and more specifically Fe_2C, is a precursor to the appearance of the graphite fibers which comprise the bulk of the reaction products. With regard to the thermal stability of Fe_2C, Nagakura (*37*) has shown that at 550°C Fe_2C and Fe_3C may indeed coexist. The following observations indicate that the most viable mechanism for the production of these fibers involves the graphitization, either thermally or by interaction with H_2, of Fe_2C whiskers almost immediately after they begin to grow from their base. Graphite fiber growth is then halted when carbide whisker growth ceases.

1. Reflections corresponding to the Fe_2C lattice were found in the selected area diffraction patterns obtained from the fibers shown in Fig. 12. This was one of the few instances found in which the carbide whiskers had not been completely broken down.

2. The whiskers visible in Fig. 18, which were identified as Fe_3C, clearly demonstrate the ability of Fe carbides to grow in whisker form.

3. It is difficult to envisage any other mechanism for the formation of fibers which consist of loosely packed crystallites radially disposed about a hollow core. In terms of the decomposition of an Fe_2C whisker the fiber porosity, which includes the hollow core, can among other things be related to the volume of the displaced Fe. The only other possible mechanism for fiber growth would involve the deposition of carbon from a catalyst particle residing at the fiber tip. Indeed in many instances the fibers do appear to be less transparent to electrons at their ends, although selected area diffraction always failed to indicate any material other than carbon at these locations. However, to produce a fiber approximately 0.3 mm long in this manner would require a relatively large catalyst particle because the latter would undoubtedly be broken down during the course of reaction. In addition, such a reduction in the particle size of the catalyst could not account for the uniform diameter displayed by the majority of the fibers.

4. Well-defined crystals of Fe_3C are found trapped within the confines of the fibers. This entrapped Fe_3C, which is a product of the thermal decomposition of Fe_2C, would explain why previous investigators (*2*, *3*) have found it difficult to remove the last traces of Fe, even by acid leaching, from the carbonaceous products.

5. The formation of graphite fibers by the decomposition of carbide whiskers is also in accord with the relatively large, considering the low formation temperature, L_a and L_c values for the graphite crystallites (*3*). In all probability the graphite

platelets, found along with the fibers in the reaction products, grew from carbide platelets such as appear in Fig. 14. It is not possible to decide whether these particular carbide platelets were a product of the decomposition of Fe_2C or rather the direct result of the interaction of carbon with the oxide.

Finally, Walker *et al.* (*3*, *4*) have shown conclusively that the build up of Fe_3C in the reaction products eventually stops the disproportionation reaction, unless sufficient H_2 is introduced to the gas stream. The breakdown of Fe_3C by H_2 presumably results in the formation of certain hydrocarbons, however, it appears that these must be unstable under the experimental conditions since the stoichiometry of the overall reaction is given by Eq. (1).

Conclusions

For Fe and Si–Fe it was found that the active catalytic species for the disproportionation of CO is a *p*-type oxide. In most instances this oxide was γ-Fe_2O_3 which was presumably stabilized at temperatures up to 600°C by an underlying Fe_3O_4 lattice. It was postulated that the cation vacancies present in the γ-Fe_2O_3 lattice provide suitable pathways for the diffusion of Fe^{3+} ions to the gas–solid interface where they can facilitate the chemisorption and eventual rupture of the CO molecule.

As a prerequisite for the formation of γ-Fe_2O_3 it was necessary for water vapor to be present in the reactants. In the absense of water vapor the outer oxide scale was α-Fe_2O_3. The rate of disproportionation over this latter oxide was considerably lower than that observed over γ-Fe_2O_3 which is commensurate with the fact that the α-Fe_2O_3 lattice contains a very much lower equilibrium concentration of point defects. Hematite was also the predominant outer oxide scale when the reaction was performed at temperatures in excess of 600°C. This observation is in good agreement with the known reduction in the disproportionation reaction rate above this temperature.

At 550°C the reaction rate was apparently controlled by the breakdown of Fe_2C. This was evident from the increased reaction rates obtained when (i) Si–Fe rather than Fe crystals were employed, (ii) the water vapor content of the gas was increased, and (iii) a CO–H_2 mixture was substituted for CO. Evidence was presented which strongly suggests that Fe_2C forms principally as whiskers and that the subsequent breakdown of these whiskers leads to the formation of the graphite fibers so characteristic of this reaction. The latter are characterized by a radial distribution of tiny crystallites about a hollow core.

Finally, despite the apparent simplicity of Eq. (1), it has been shown that the disproportionation of CO is a complex reaction. Although the various stages involved in the reaction have been identified, in many cases, because of the number of possibilities for reaction, the precise pathway for each stage still remains a matter for conjecture.

References

1. Berry, T. F., Ames, R. N., and Snow, R. B., *J. Amer. Ceram. Soc.* **39**, 308 (1956).
2. Taylor, J., *Iron Steel Inst., London* **184**, 1 (1956).
3. Walker, P. L., Jr., Rakszawski, J. F., and Imperial, G. R., *J. Phys. Chem.* **63**, 133 (1959).
4. Walker, P. L., Jr., Rakszawski, J. F., and Imperial, G. R., *J. Phys. Chem.* **63**, 140 (1959).
5. Haas, L. A., Khalafalla, S. E., and Weston, P. L., *Bur. Mines (U. S.) Rep. Invest.* **7064**, (1968).
6. Donald, H. J., An Annotated Bibliography, Mellon Inst. Res., 1956.
7. Hochman, R. F., *Proc. Div. Refining, Amer. Petrol. Inst.*, **46**, 331 (1966).
8. Boudouard, O., *Ann. Chim. Phys.* **24**, 5 (1901).
9. Hilpert, S., and Dieckmann, T., *Chem. Ber.* **48**, 1281 (1915).
10. Hofmann, U., and Groll, E., *Z. Anorg. Allg. Chem.* **191**, 414 (1930).
11. Tutiya, H., *Sci. Pap. Inst. Phys. Chem. Res.*, Tokyo **10**, 69 (1929).
12. Olmer, F., *J. Phys. Chem.* **46**, 405 (1942).
13. Baukloh, W., and Edwin, B., *Arch. Eisenhuettenw.* **16**, 197 (1942).
14. Fleureau, B., *C. R. Acad. Sci.*, **237**, 330 (1953).
15. Chatterjee, B., and Das, P. P., *Nature (London)* **173**, 1046 (1954).

16. MacRae, D. R., presented: *Annu. Meet. Amer. Inst. Mining Eng.*, New York, March, 1966.
17. Ruston, W. R., Warzee, M., Hennaut, J., and Waty, J., *Carbon (Oxford)* **7**, 47 (1969).
18. Trillat, J. J., and Oketani, S., *C. R. Acad. Sci.* **230**, 2203 (1950).
19. Trillat, J. J., and Oketani, S., *C. R. Acad. Sci.* **233**, 51 (1951).
20. Kehrer, V. J., and Leibheiser, H., *J. Phys. Chem.* **58**, 550 (1954).
21. Suits, J. C., and Low, J. R., *Acta Met.* **5**, 285 (1957).
22. Morris, C. E., *Metal Progr.* **56**, 696 (1949).
23. David, I., and Welch, A. J. E., *Trans. Faraday Soc.* **52**, 1942 (1956).
24. Boggs, W. E., Kachik, R. H., and Pellissier, G. E., *J. Electrochem. Soc.* **114**, 32 (1967).
25. Gazzarini, F., and Lanzavecchia, G., *in* "Reactivity of Solids" (J. W. Mitchell, R. C. DeVries, R. W. Roberts, and P. Cannon, eds.), p. 57. Wiley (Interscience), New York, 1969.
26. Hofer, L. J. E., Sterling, E., and McCartney, J. T., *J. Phys. Chem.* **59**, 1153 (1955).
27. David, W. R., Slawson, R. J., and Rigby, G. R., *Nature (London)* **171**, 756 (1953).
28. Jack, K. H., *Proc. Roy. Soc. Ser., A* **195**, 56 (1948).
29. Ron, M., Shechter, H., and Niedzwiedz, S., *J. Appl. Phys.* **39**, 265 (1968).
30. Milavsky, A. I., and Weinstein, M., *J. Appl. Phys.* **34**, 2885 (1963).
31. Columbo, U., Gazzarini, F., and Lanzavecchia, G., *Mater. Sci. Eng.* **2**, 125 (1967).
32. Pinsker, Z. G., "Electron Diffraction," p. 108. Butterworths, London, 1953.
33. Baird, T., and Dawson, I. M., *U. K. At. Energy Auth., Reactor Group, TRG Report* **1924** (c/x), (1967).
34. Kachi, S., Momiyama, K., and Shimizu, S., *J. Phys. Soc. Jap.* **18**, 106 (1963).
35. Takei, H., and Chiba, S., *J. Phys. Soc. Jap.* **21**, 1255 (1966).
36. Baraniecki, C., Pinchbeck, P. H., and Pickering, F. B., *Carbon (Oxford)* **7**, 213 (1969).
37. Nagakura, S., *J. Phys. Soc. Jap.* **14**, 186 (1959)